IEEE Access
Multidisciplinary ⋮ Rapid Review ⋮ Open Access Journal

Received 18 June 2023, accepted 5 July 2023, date of publication 19 July 2023, date of current version 28 July 2023.

Digital Object Identifier 10.1109/ACCESS.2023.3296804

RESEARCH ARTICLE

Fast Method for the Assessment of SRR or ELC-Based Planar Filters: Numerical Analysis and Experiments

M. ALDRIGO[1], (Senior Member, IEEE), L. ZAPPELLI[2], (Member, IEEE), A. CISMARU[1], M. DRAGOMAN[1], S. IORDANESCU[1], (Life Member, IEEE), D. MLADENOVIC[1], C. PARVULESCU[1], D. VASILACHE[1], C. H. JOSEPH[2], (Member, IEEE), D. MENCARELLI[2], (Member, IEEE), L. PIERANTONI[2], (Senior Member, IEEE), AND P. RUSSO[2], (Member, IEEE)

[1]National Institute for Research and Development in Microtechnologies, IMT-Bucharest, 077190 Voluntari, Ilfov, Romania
[2]Dipartimento di Ingegneria dell'Informazione, Università Politecnica delle Marche, 60131 Ancona, Italy

Corresponding author: L. Zappelli (l.zappelli@univpm.it)

This work was supported in part by the European Project H2020 FETOPEN-01-2018-2019-2020 "NANOPOLY" under Grant 829061; in part by the European Project Horizon Europe HORIZON-EIC-2022-TRANSITIONCHALLENGES-01 "SMARTWAY" under Grant 101103057; in part by the Romanian Ministry of Research, Innovation and Digitalization, Colegiul Consultativ pentru Cercetare-Dezvoltare și Inovare (CCCDI)-Unitatea Executivă pentru Finanțarea Învățământului Superior, a Cercetării, Dezvoltării și Inovării (UEFISCDI), within Planul Național de Cercetare Dezvoltare și Inovare (PNCDI) III, under Project PN-III-P4-PCE-2021-0223; and in part by the Core Program within the National Research Development and Innovation Plan 2022-2027, carried out with the support of Ministerul Cercetării, Inovării şi Digitalizării (MCDI)), under Project 2307.

ABSTRACT We present a general-purpose, fast and computationally efficient numerical method to predict the performance of filters based on electric-LC (ELC) resonators or split-ring resonators (SRR) in a very large frequency range (i.e., 8–40 GHz). In particular, we tackle the problem arising from the design of arrays of ELC/SRR-based resonators developed in a multi-layer dielectric stack under a coplanar waveguide excitation. The intrinsic complexity of the analyzed structure (open, multi-layer, and with resonators) makes it unpractical to rely exclusively on full-wave electromagnetic simulations. Furthermore, the presence of multiple modes in propagation can lead to a quite difficult assessment of the optimal simulation conditions. For all these reasons, we propose a method based on the cascade of scattering matrices for all the sub-modules of the considered filters. We demonstrate the efficacy of the proposed numerical technique for a good prediction of the high-frequency performance of the filters. The fabrication on silicon substrate of structures integrating electric-LC resonators (for X band applications) or split-ring resonators (for Ka band applications) serves the purpose of validating the presented method, with a very good agreement between simulations and measurements.

INDEX TERMS Electromagnetic modeling, planar resonators, microwave filters, numerical analysis, numerical modeling.

I. INTRODUCTION

In the current panorama of wireless communications, the spectrum allocation assigns specific frequency ranges to different applications. In particular, the X, Ku, K, and Ka bands covering the band 8.2–40 GHz are of great importance for space communications, radar systems, terrestrial links, and for ISM 24 GHz telecommunications systems. A key aspect is the development of devices that are complementary metal-oxide-semiconductor (CMOS) compatible, as this ensures a large-scale fabrication for high-volume commercialization. Hence, the design, fabrication, and experimental characterization of silicon-based devices and components becomes compelling.

In this scenario, split-ring resonators (SRR), electric-LC (ELC) resonators, and their complementary designs have

The associate editor coordinating the review of this manuscript and approving it for publication was Guido Lombardi.

been used within planar transmission lines, such as coplanar waveguides (CPWs) and microstrip lines, to improve the performance of the microwave/millimeter-wave components for broadband applications [1], [2], [3]. ELC resonators display high symmetry and a strong coupling with the electric field, showing negative permittivity at resonance. On the other hand, SRRs with two splits couple strongly with the magnetic field, acting like a magnetic-LC resonator and showing negative permeability at resonance [4], [5]. These sub-wavelength resonator elements in combination with stubs or gaps has been utilized to design different kinds of filters [6]. Such filters have been designed/optimized using a variety of numerical, circuit, or commercial electromagnetic simulators [7], [8], [9], [10]. These components can be also used to obtain sub-wavelength elementary building blocks (or ''meta-atoms''), which can be combined in a periodic shape to obtain the so-called ''metasurfaces'' that can be exploited to obtain ''unusual'' electromagnetic (EM) properties, which are not to be found in natural materials [11], [12]. Consequently, completely new applications in the vast EM spectrum, from sensing, shielding, energy harvesting, to wavefront shaping and beam steering [13], [14], [15], [16], [17] are possible. Within this landscape of vast potentialities, metasurface-based applications related to actual and future wireless communication systems [18], [19], [20] have emerged as promising candidates to realize new technological paradigms also for the upcoming 6G networks [21], [22].

In this work, we propose an accurate and fast numerical method to assess the global behavior of high-frequency silicon devices integrated with two-dimensional (2D) meta-atoms, ELCs or SRRs, to create stop-band and high-pass filters working from 8 up to 40 GHz. The use of CPW lines, when loaded with 2D meta-atoms on a high-permittivity substrate, gives rise to a huge complexity in analyzing the resulting components with a three-dimensional (3D) EM simulation tool. The calculation time, even in a workstation, can become unfeasible if one needs an accurate solution. Moreover, as it will be shown in the following, the designer must also consider multi-mode excitation in presence of thick high-permittivity substrates, which further complicates the analysis of the structures under test, especially if higher order modes propagate besides the fundamental one. All these issues will be tackled in depth throughout the paper, and the final result is a general-purpose compact method to predict the performance of the proposed filters in a time much shorter than that necessary with a numerical commercial electromagnetic simulator, thus leaving space to a time-efficient optimization.

The paper is organized as follows: first, we present the theory upon which the proposed numerical approach relies, together with the analysis of ELC or SRR-based filters on silicon; then, we provide some details about the fabrication of test structures for the validation of the numerical method; last, a thorough comparison among the 3D EM simulations, the optimized numerical simulations, and the experiments is discussed to validate the initial hypothesis.

II. THEORY AND DESIGN

One of the issues in using 3D EM simulation tools for the design of components integrating planar ELC/SRR-based meta-atoms is the number of steps necessary to fulfil the desired (expected) specifications, e.g., in terms of scattering parameters. In fact, the number of simulations increases with the number of geometrical parameters involved in the optimization of the structure under study. In this respect, one could use some numerical ''tricks'' to partially overcome this problem. A possible choice is to define some equivalent circuits of the meta-atoms contained in the structure, to derive an overall equivalent circuit containing the dependence from the geometric parameters [23]. Unfortunately, this approach could not be efficient because the equivalent circuits are often defined only in a very narrow bandwidth, for example near a resonance, or they are not defined at all. A more efficient strategy, which is precisely what we propose in this paper, is based on the application of the microwave networks theory, typical for closed structure: the overall device is subdivided into a cascade of meta-atoms, whose scattering matrices are derived using a numerical tool. With this approach, it is not necessary to extract an equivalent circuit of the single meta-atom over the whole analyzed band, which could be very complex, especially if losses or a multi-mode propagation must be taken into account. We need only the $(N_1 + N_2) \times (N_1 + N_2)$ scattering matrix S that represents the whole property of the single device, with N_1 input and N_2 output ports (modes), hence without the need to define a very complex equivalent circuit.

The structures considered in this paper are based on ELC/SRR meta-atoms developed in a multi-layer dielectric stack under a CPW excitation. It should be noted that the proposed approach is general-purpose and, hence, can be applied to any other type of excitation, such as microstrip or plane wave. The meta-atoms placed along the direction of propagation of the EM field, let's say z in our case, can be analyzed by evaluating the scattering matrix S of each meta-atom, seen as a discontinuity placed between two cross-sections, corresponding to the input and output ports of this discontinuity. If only the TEM mode is in propagation, as it usually happens at frequencies that are not too high with respect to the substrate thickness, the related S-matrix has dimensions 2×2. The global representation of the cascade of the meta-atoms can be obtained by cascading the scattering matrices S of the single meta-atoms, in the hypothesis that the interaction between evanescent higher order modes is negligible. The S-matrix cascade, S^c, between two successive 2×2 S-matrices, let's say S^a and S^b, is given by $S^c = S^a * S^b$, as follows [24, Ch. A.4]:

$$S_{11}^c = S_{11}^a + \frac{S_{12}^a S_{21}^a S_{11}^b}{1 - S_{22}^a S_{11}^b} \tag{1}$$

$$S_{12}^c = \frac{S_{12}^a S_{12}^b}{1 - S_{22}^a S_{11}^b} \tag{2}$$

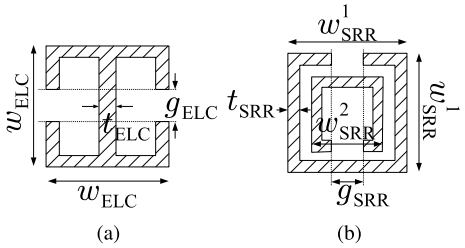

FIGURE 1. Geometry of the meta-atoms: (a) ELC; (b) SRR.

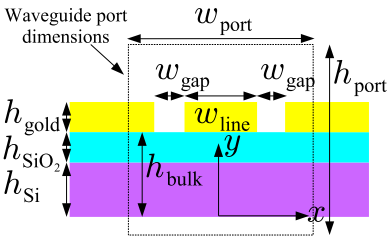

FIGURE 2. Transverse section (not in scale) of the CPW.

$$S_{21}^c = \frac{S_{21}^a S_{21}^b}{1 - S_{22}^a S_{11}^b} \tag{3}$$

$$S_{22}^c = S_{22}^b + \frac{S_{22}^a S_{21}^b S_{12}^b}{1 - S_{22}^a S_{11}^b}. \tag{4}$$

The S cascade drastically reduces the simulation time of the overall device (made by many meta-atoms), with respect to that required by any EM simulation tool based on some numerical method in the time or frequency domain. In fact, the S-matrix of each meta-atom is evaluated only once by the EM simulation tool, while the optimization in terms of distance between succesive meta-atoms can be made by cascading the meta-atoms' S-matrices by using a numerical software such as Mathematica, Matlab, Octave, etc. The simulation time of the optimization process is surely shorter than that required by the EM simulator for the overall device. It should be noted that this approach is very adaptable. In fact, if we are able to collect a database of meta-atoms with different geometries in terms of their S-matrices, we can satisfy the requirements on the global S-matrix by means of a simple mathematical technique that optimizes not only the distance between the meta-atoms in the direction of propagation but also different geometries for each meta-atom in the transverse section.

This approach has been used in the optimization process for closed waveguide devices but the question that arises is the following: can it be applicable also to open waveguides as well, e.g., coplanar- and microstrip-based structures? The answer could be positive but some remarks must be done. There are at least two problems to tackle in addressing this fundamental issue:

1) it is not sure that the cascade of two S-matrices, each one referring to an open structure, gives the correct results, because the two devices, placed at a certain distance along the direction of propagation of the EM field, could interact by means of the power radiated by each of them in a similar way to what happens for higher order modes in closed waveguides.
2) The use of an EM simulation tool to characterize a scattering matrix usually requires the definition of a spatially limited port that must enclose the "main" part of the EM field. In an open waveguide the field extends to infinity and an incorrect choice of the port dimensions could introduce errors in the evaluation of the scattering matrix.

The first problem could be solved by placing at a proper longitudinal distance two successive meta-atoms, for example the pairs of SRRs or ELCs shown in Fig. 1a-1b, or other metasurface-like devices. Unfortunately, it is not possible to establish "a priori" a minimum distance because we cannot represent the radiated power as "higher order modes" but as a continuous spectrum of radiated waves, as usually occurs in open dielectric waveguide [25, Ch. 14] and we cannot evaluate a decay law for the radiated power permitting us to define such minimal distance between the meta-atoms. Hence, even if we cannot extract an equation for the minimal distance between two successive meta-atoms to be sure that the simulations with the cascade approach give a very good approximation, we can obtain a thumb rule in terms of wavelength, which ensures that an optimization process on the distance and/or number of the meta-atoms, based on the cascade approach, can be a winning strategy, thus validating the initial hypothesis. Even in presence of multi-mode propagation in the CPW, for example due to a thick substrate, the cascade approach is still valid to obtain a fair prediction of the global results, as it will be demonstrated in the following results.

The second problem is more complex and it is strictly related to the geometry of the device under test, which is supposed to be realized in coplanar waveguide, whose cross-section is shown in Fig. 2, where Si indicates the silicon substrate and SiO_2 a thin layer of silicon oxide thermally grown on the Si wafer. For example, noticeable differences can be observed in the suitable ports defined in the following two situations: a pair of ELCs/SRRs (symmetric with respect to the z axis) is placed (i) either in the back plane of a multilayer structure, as in Fig. 3a, (ii) or in the plane of the CPW, between the signal line and the ground plane(s), as shown in Fig. 3b-3c. The differences are related to the device under test (DUT), the frequency range we are considering, the distance between the ground and line conductors, and the substrate thickness.

A careful analysis of the definition of the ports and of the number of modes taken into account must be done to obtain a reliable scattering matrix of the DUT. In fact, it should be recalled that the evaluation of an S-matrix with a numerical tool requires the use of spatially limited ports within a contour path, i.e. the "waveguide port" shown in Fig. 2, with proper enforcing boundary conditions that are used to evaluate the

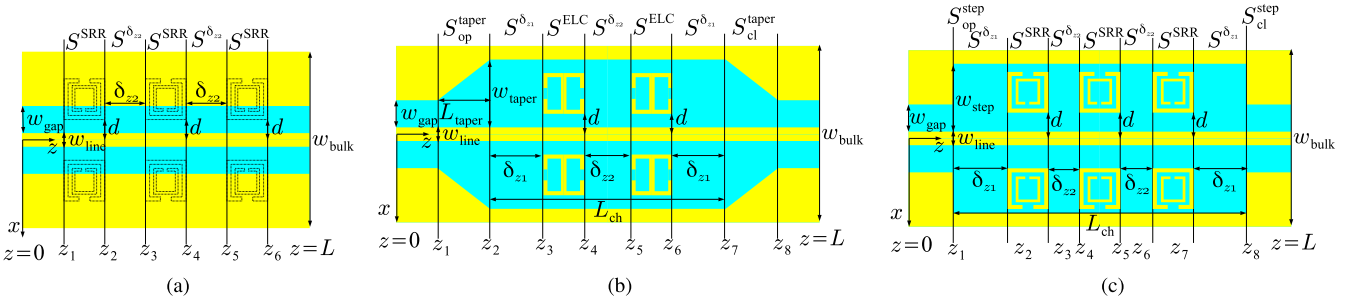

FIGURE 3. Meta-atom based filters in coplanar waveguide technology: (a) SRR bottom placement; (b)-(c) ELC/SRR top placement.

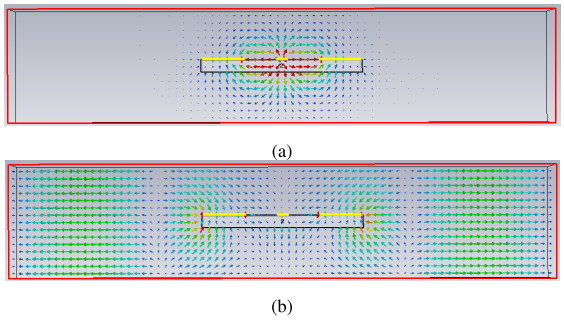

FIGURE 4. Transverse electric field in a CPW delimited by a "numerical" waveguide port: (a) Quasi-TEM mode and (b) "numerical" mode. The line and ground conductors are highlighted in yellow.

modes associated to that port. This spatial limitation is in contrast with the "nature" of the CPW that is an open waveguide. Hence, the dimensions of the port must ensure at the same time (a) a very low intensity of the EM field along the contour path of the port, and (b) that no fictitious ("numerical") higher order modes start propagating in the frequency range of interest due to the dimensions of the port. The transverse electric field distribution of a "numerical" mode is shown in Fig. 4 together with the "true" Quasi-TEM mode. The presence of the fictitious mode is due to the choice of a too wide lateral dimension of the port. The actual guided modes of an open waveguide, as the CPW, are characterized by one, or more, maxima of the electromagnetic field always confined within the dielectric, as shown in Fig. 4a for the "true" Quasi-TEM mode, and never in the air surrounding the dielectric substrate [25, Ch. 14]. On the other hand, the "numerical" mode is characterized by the presence of a stationary wave with maxima of the electromagnetic field outside the substrate related to the choice of a too wide lateral dimension of the port, as shown in Fig. 4b. Hence, the presence of "numerical" modes must be avoided by a proper choice of the waveguide port dimensions.

In the following sub-sections, we will analyze the different problems that can arise in the design of filters by choosing different meta-atoms (ELCs or SRRs), changing their placement on the dielectric bulk substrate, and analyzing also the effect of the frequency band with respect to the bulk thickness. The chosen filters are shown in Fig. 3a-3c and they have been simulated using CST Microwave Studio® but the proposed method is valid for any other 3D EM tool using a time or frequency domain approach (such as HFSS®, COMSOL®, etc.).

A. SRRs IN THE BOTTOM PLANE

For the filter shown in Fig. 3a, where the pair of SRRs is placed in the bottom surface, the overall S-matrix is obtained with the cascade of five blocks: $S^{\text{tot}} = S^{\text{SRR}} * S^{\delta_{z2}} * S^{\text{SRR}} * S^{\delta_{z2}} * S^{\text{SRR}}$. S^{SRR} is the S-matrix of the pair of SRRs and $S^{\delta_{z2}}$ is the S-matrix of an unperturbed CPW with length δ_{z2}. Being the EM field configuration of the CPW always the same along the direction of propagation, both scattering matrices are referred to the same kind of port, defined in the transverse plane as a rectangle, symmetrically placed with respect to the z-axis, as shown in Fig. 2, confining as much as possible the EM field. This last condition can be met considering the horizontal dimension of the rectangle equal to $w_{\text{port}}^{\text{cpw}} = k_x^{\text{cpw}}(w_{\text{line}} + 2w_{\text{gap}})$, with $3 \leq k_x^{\text{cpw}} \leq 5$. S^{SRR} is calculated with CST while $S^{\delta_{z2}}$ is characterized by the propagation constant of the fundamental Quasi-TEM mode β_{TEM}, evaluated with respect to the previously defined waveguide ports. For example, setting $\delta_{z2} = z_3 - z_2$ for the section between z_2 and z_3 in Fig. 3a, we can write

$$S^{\delta_{z2}} = \begin{bmatrix} 0 & e^{-j\beta_{TEM}\delta_{z2}} \\ e^{-j\beta_{TEM}\delta_{z2}} & 0 \end{bmatrix}. \tag{5}$$

The propagation constant β_{TEM} can be also extracted with CST and used to evaluate $S^{\delta_{z2}}$ as in (5). Consequently, for this case, the calculation of the global S-matrix is simple: since all scattering matrices refer to the same DUT depicted in Fig. 3 with identical meta-atoms, only one evaluation must be done with CST, i.e., the pair of SRRs placed between z_1 and z_2.

The proposed approach has been applied to the case of pairs of SRRs placed in the bottom plane with $h_{\text{Si}} = 0.25$, $h_{\text{SiO}_2} = 0.0003$, $h_{\text{gold}} = 0.0005$, $w_{\text{line}} = 0.3$, $w_{\text{gap}} = 0.19$, $d = 0.25$, $w_{\text{bulk}} = 7.74$, $g_{\text{SRR}} = 0.1$, $t_{\text{SRR}} = 0.02$, $w_{\text{SRR}}^1 = 1.03$, $w_{\text{SRR}}^2 = 0.79$ (all dimensions are in millimeter throughout the paper), $\varepsilon_{\text{r,Si}} = 11.9$, $\sigma_{\text{Si}} = 0.01$ S/m, and $\varepsilon_{\text{r,SiO}_2} = 3.7$. It has to be stressed here that in all the analyzed structures, the bulk substrate has been considered

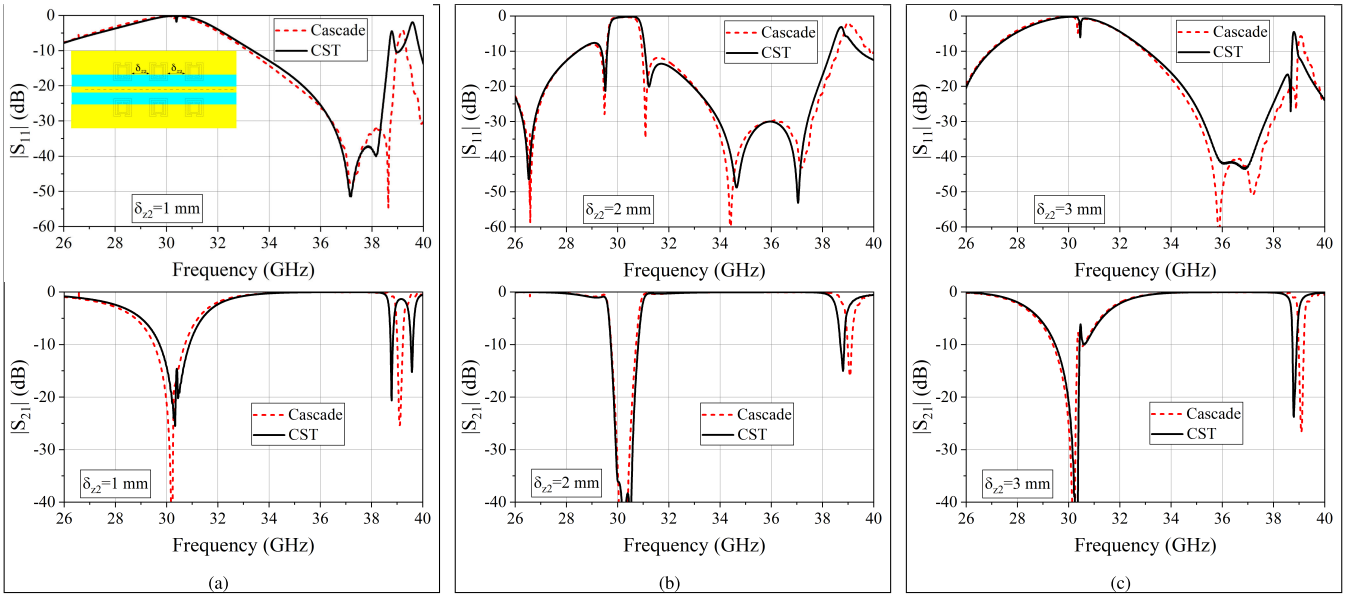

FIGURE 5. $|S_{11}|$ and $|S_{21}|$ for three bottom pairs of SRRs, as shown in the inset or enlarged in Fig. 3a. Black lines refer to the cascade of the S-matrices and red lines refer to the CST simulations for the whole structure, for various z-distances, δ_{z2}, between pairs of SRRs.

in the simulations as if it were of finite width. The scattering parameters S^{SRR} for one bottom pair of SRRs have been evaluated with CST and the interested reader can found them in Appendix A, Fig. 19. They are used to evaluate the global S-matrix for a combination of two bottom pairs of SRRs placed at a variable distances δ_{z2} to evaluate the minimum distance that ensures a good comparison between the cascade approach and the global CST evaluation. An initial choice could be to set δ_{z2} equal to a fraction of the wavelength of the Quasi-TEM mode evaluated at the resonance of the pairs of SRRs, say λ_{res}, that occurs, in our case, at about 30.2 GHz (Fig. 19): $\lambda_{\text{res}} \approx 4$ mm. If we choose $\frac{\delta_{z2}}{\lambda_{\text{res}}} = 0.1, 0.2, 0.3, \ldots$, we can compare the results obtained with CST and the cascade approach. From those evaluations, not reported here for brevity, we have set the minimum distance to $\delta_{z2}/\lambda_{\text{res}} = 0.25$, corresponding to $\delta_{z2} = 1$ mm. Now we can apply the minimum distance to more complex structures with more pairs of SRRs, just three as shown in Fig. 3. The results obtained with the cascade of S^{SRR} and $S^{\delta_{z2}}$ are shown in Fig. 5 for $\delta_{z2} = 1, 2, 3$ mm and they are compared with the S parameters derived with a global evaluation of the corresponding structure with CST. The comparison is very good apart from a minimal difference in the upper part of the considered frequency range, where the effect of the radiating spectrum could appear. Moreover, the comparison is very good also for values of $\delta_{z2} > 3$ mm, not reported here for brevity. It should be noted that the analyzed filter and the obtained minimum distance can be used to "rescale" the filter geometry to analyze a similar structure in a different bandwidth. For example, if we "rescale" the geometry of the filter by a factor 3 (i.e. all dimensions are multiplied by 3), we obtain a pair of SRRs resonating at about 10 GHz.

TABLE 1. Run time comparison for three bottom pairs of SRRs.

Case	Cascade Approach Run Time	CST Run Time
S^{SRR} (Fig. 19)	1h 35m (with CST)	
Fig. 5a	3 s	5h 50m
Fig. 5b	3 s	6h 20m
Fig. 5c	3 s	6h 40m
whole Fig. 5	1h 35m (S^{SRR}) + 9 s (Fig. 5a-c)	18h 50m

If we choose the same relative minimum distance $\delta_{z2}/\lambda_{\text{res}} = 0.25$ at 10 GHz ($\delta_{z2} \approx 3.04$ mm), we obtain again that the cascade approach yields to numerical results that are in a very good comparison with those obtained by a global simulation with CST.

The global run time for the cascade approach and the CST simulations are shown in Tab. 1. It is quite clear that the main run time in the cascade approach is the simulation of the S-matrix S^{SRR} of one pair of SRRs alone (1h 35m), while the run time to obtain each sub-figure of Fig. 5 is about 3s by using a self-developed code in Wolfram Mathematica©. On the contrary, the simulation with CST of each case of the same figure requires more than 6h. Hence, it its evident that the cascade approach can be an efficient and fast numerical approach in the optimization of a filter based on pairs of SRRs placed on the back of the substrate. In fact, any optimization process requires tens of simulations that can be very time-consuming if performed with an electromagnetic simulator. In the proposed cascade approach, the main (and only) time-consuming step is just the evaluation of the S-matrix of the meta-atom (first row of Tab. 1).

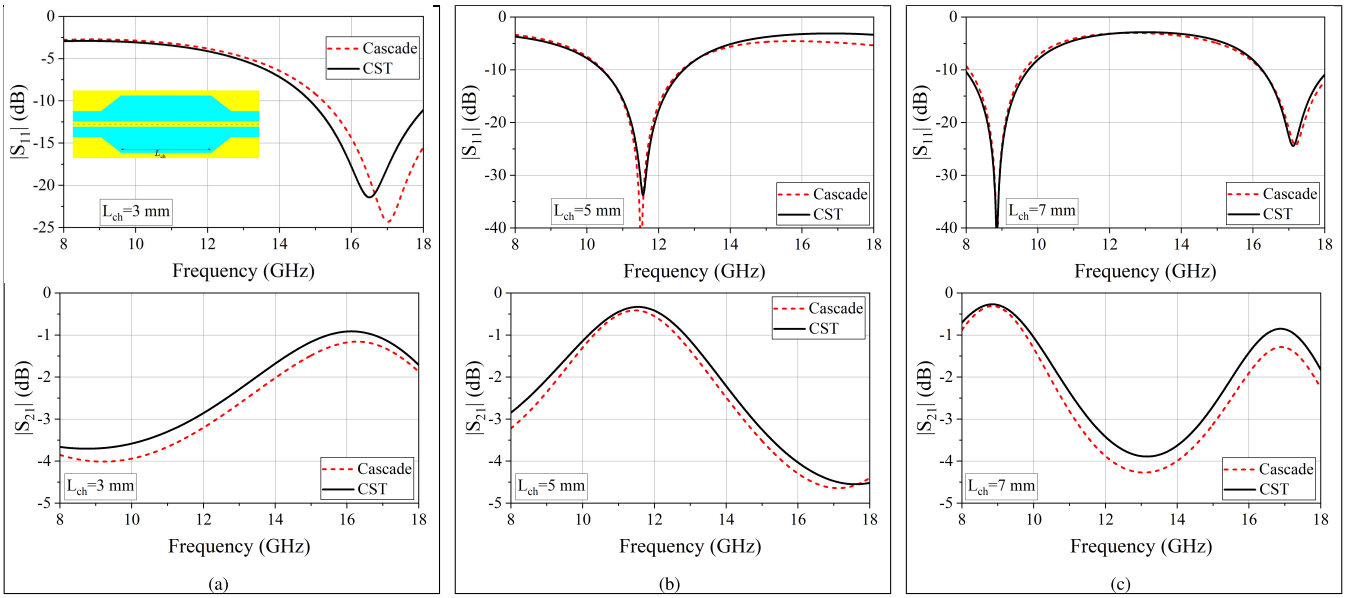

FIGURE 6. $|S_{11}|$ and $|S_{21}|$ comparison between cascade approach and CST evaluations for the double taper structure shown in the inset or enlarged in Fig. 3b, by varying the length L_{ch} of the channel.

B. ELCs IN THE TOP PLANE FOR X AND KU BAND APPLICATIONS

For the filter shown in Fig. 3b, the ELC meta-atoms have been chosen and placed on the top plane. This arrangement requires that the CPW gap is enlarged to permit the insertion of the meta-atoms.

The analysis of this geometry requires the use of seven cascading blocks and the global S-matrix is given by (see Fig. 3b): $S^{\text{tot}} = S_{\text{op}}^{\text{taper}} * S^{\delta_{z1}} * S^{\text{ELC}} * S^{\delta_{z2}} * S^{\text{ELC}} * S^{\delta_{z1}} * S_{\text{cl}}^{\text{taper}}$. However, only three matrices have to be calculated: $S_{\text{op}}^{\text{taper}}$, S^{ELC}, $S^{\delta_{z2}}$. In fact, the matrix $S_{\text{cl}}^{\text{taper}}$ of the "closing" taper between z_7 and z_8 is the reverse of the"opening" taper matrix, $S_{\text{op}}^{\text{taper}}$, between z_1 and z_2, for they are geometrically symmetric blocks. Its values can be easily obtained inverting the order of ports of the $S_{\text{op}}^{\text{taper}}$ matrix.

The main problem is that in this case the S-matrices refer to two different types of ports, the first being defined at $z = 0$ (or $z = z_1$) and the second at $z = z_2$. In both cases, as seen in the previous section, the horizontal dimension of the rectangular port depends on the width of the CPW signal line w_{line} and on the width of the gap w_{gap}. But, while the size $w_{\text{port}}^{\text{cpw}} = k_x^{\text{cpw}}(w_{\text{line}} + 2w_{\text{gap}})$ with $3 \leq k_x^{\text{cpw}} \leq 5$ guarantees the propagation of the fundamental mode only and at the same time the confinement of the whole field within it, the size of the second port $w_{\text{port}}^{\text{taper}} = k_x^{\text{taper}}(w_{\text{line}} + 2w_{\text{taper}})$ with $3 \leq k_x^{\text{taper}} \leq 5$ can become so large that "numerical" higher modes can appear. The propagation of the sole Quasi-TEM mode is strictly related to the height of the dielectric substrate with respect to the considered frequency range. If the height of the substrate is sufficient to ensure propagation of higher order modes, the choice of the port dimensions becomes more decisive, as will be discussed in the next subsection. Hence, the definition of the port dimensions is crucial to obtain correct results from the physical point of view.

As an example of the application of the previous approach, let us consider the structure shown in Fig. 3b working in the frequency range 8–18 GHz (X and Ku bands). Referring to Fig. 1a for the ELC and to Fig. 3b for the device, the analyzed structure has the following dimensions: $w_{\text{line}} = 0.3$, $w_{\text{gap}} = 0.19$, $w_{\text{taper}} = 2.34$, $L_{\text{taper}} = 0.85$, $w_{\text{bulk}} = 7.74$, $h_{\text{Si}} = 0.525$, $w_{\text{ELC}} = 1.55$, $t_{\text{ELC}} = 0.15$, $g_{\text{ELC}} = 0.15$, and $d = 0.275$. We must evaluate $S_{\text{op}}^{\text{taper}}$, which is comprised between two sections with two different port sizes. If we consider for both ports a horizontal ratio $k_x^{\text{cpw}} = k_x^{\text{taper}} = 4$, the frequency band and the height of the substrate ensure the propagation of the fundamental mode only without any "numerical" mode. For this case, we can evaluate with CST the S-matrices $S_{\text{op}}^{\text{taper}}$ and S^{ELC} without any problem, being the size of the ports at $z = z_1, z_2, z_3, z_4$ well defined to ensure a correct representation of the Quasi-TEM mode behavior. The interested reader can found the plot of the S parameters of the opening taper, $S_{\text{op}}^{\text{taper}}$, and of one pair of ELCs, S^{ELC}, in Appendix B, Figs. 20a and 20b.

The evaluated $S_{\text{op}}^{\text{taper}}$ is at first used to simulate the structure shown in Fig. 3b without the ELC resonators (see the inset in Fig. 6a) by varying the length of the channel L_{ch} between the "opening" and "closing" tapers, to verify the correctness of the cascade approach. The comparison between the scattering parameters obtained with the cascade approach and the simulation of the overall structure with CST is shown in Fig. 6. The agreement seems very good, except for very small values of the channel length, L_{ch}, where the effect of coupling between evanescent higher order modes can be appreciable.

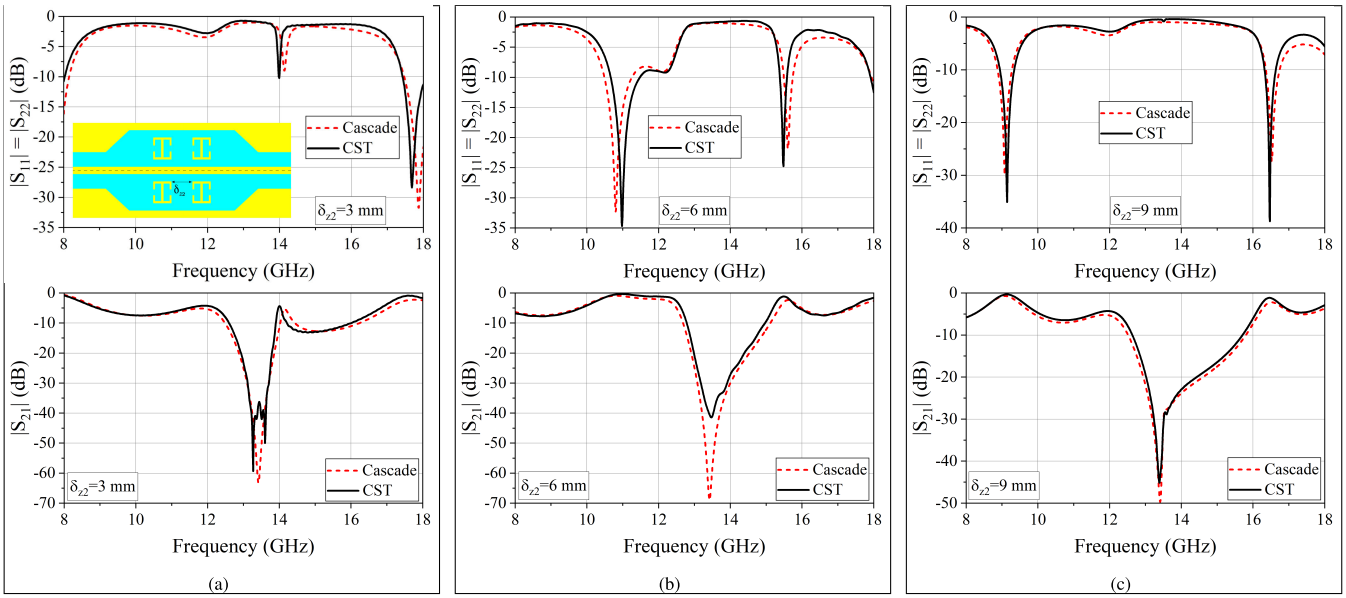

FIGURE 7. $|S_{11}|$ and $|S_{21}|$ comparison between cascade approach and CST evaluations for the structure shown in the inset or enlarged in Fig. 3b, with $\delta_{z1} = 5$ mm and two pairs of ELCs, by varying the space δ_{z2} between them.

The evaluated $S_{\text{op}}^{\text{taper}}$ and S^{ELC} are used in the cascade of scattering matrices to obtain the global scattering matrix for a combination of two pairs of ELCs with $\delta_{z1} = 5$ mm and by varying the distance $\delta_{z2} = 3, 6, 9$ mm between the pairs of ELCs (see the inset in Fig. 7 or Fig. 3b). The corresponding results are shown in Fig. 7 (dashed red lines) and they are compared with the global scattering parameters obtained by a direct evaluation of the corresponding global structure with CST (solid black line). The comparison is very good apart from a minimal mismatch in the $|S_{11}|$ resonances. From the results shown in Fig. 7, we can assume that a very good comparison is obtained at just $\delta_{z2} = 3$ mm. Hence, the minimum distance between the pairs of ELCs ensuring that the cascade approach is a winning strategy in an optimization process for this kind of filter can be set to $\delta_{z2}/\lambda_{\text{res}} = 0.34$ at the resonant frequency of one pair of ELCs, i.e. about 13.4 GHz (Fig. 20b). The run time required with the cascade approach and the CST simulations is shown in Tab. 2. The main run time for the cascade approach is due to the evaluation of $S_{\text{op}}^{\text{taper}}$ and S^{ELC} with CST, while the run time for each cascade is negligible. The minimum time required by a CST direct evaluation of each case discussed in Fig. 7 is about 2h (the run time of the first two rows in Tab. 2 refers to the cascade approach only and they must not to be taken into account in a direct evaluation with CST of Fig. 7a-c). It is evident that the cascade approach exhibits a good performance in terms of run time if applied to an optimization process of the distance between two, or more, pairs of ELCs, which requires at least tens of simulations, each of ones performed in about 3 s.

However, a major problem can arise when going up in frequency, as we will explain in the next subsection II-C.

TABLE 2. Run time comparison for the structure with two ELC resonators (Fig. 7).

Case	Cascade Approach Run Time	CST Run Time
$S_{\text{op}}^{\text{taper}}$ (Fig. 20a)	1h 35m (with CST)	
S^{ELC} (Fig. 20b)	2h 20m (with CST)	
Fig. 7a	3 s	1h 57m
Fig. 7b	3 s	4h 09m
Fig. 7c	3 s	8h 5m
whole Fig. 7	3h 55m ($S_{\text{op}}^{\text{taper}}$+$S^{\text{ELC}}$) + 9 s (Fig. 7a-c)	14h 8m

C. SRRs IN THE TOP PLANE FOR KA BAND APPLICATIONS

We have chosen to analyze in the Ka band the presence of proper designed pairs of SRRs in the top plane, replacing the pairs of ELCs with pairs of SRRs and placing an abrupt step in place of the taper, as shown in Fig. 3c. The SRRs have the same dimensions as the bottom case discussed in Section II-A except for $w_{\text{step}} = 1.32$ mm. The overall scattering matrix for this case is $S^{\text{tot}} = S_{\text{op}}^{\text{step}} * S^{\delta_{z1}} * S^{\text{SRR}} * S^{\delta_{z2}} * S^{\text{SRR}} * S^{\delta_{z2}} * S^{\text{SRR}} * S^{\delta_{z1}} * S_{\text{cl}}^{\text{step}}$, where $S_{\text{op}}^{\text{step}}$ is the scattering matrix of the "opening" step, $S_{\text{cl}}^{\text{step}}$ for the "closing" step, obtained by inverting the port of $S_{\text{op}}^{\text{step}}$ and S^{SRR} that for the pairs of SRRs.

Two ports with different dimensions can be found at $z = 0$ and $z = z_1^+$, but the analyzed frequency band suggests to perform a modal analysis of both ports. Three actual (not "numerical") higher order modes, in addition to the Quasi-TEM fundamental mode, are propagating in the large CPW at $z = z_1$ with the previous dimensions in the chosen frequency band. The modal analysis of the higher order modes

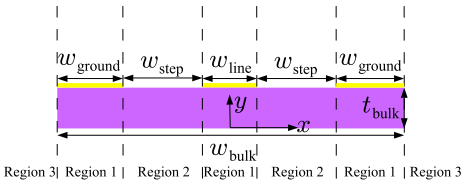

FIGURE 8. Definition of the regions of the transverse section used in the EDC analysis for the large CPW at $z = z_1$ in the filter shown in Fig. 3c.

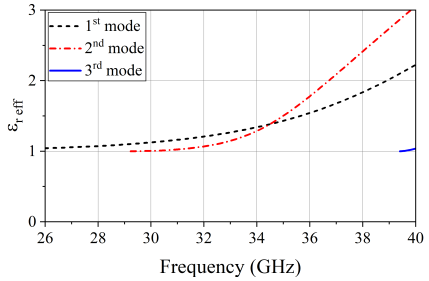

FIGURE 9. Effective dielectric constant $\varepsilon_{r,eff}$ of the higher order modes for the large CPW obtained by the EDC method.

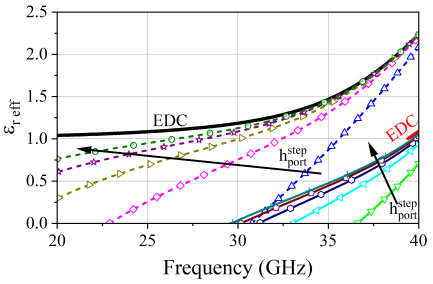

FIGURE 10. Variation of $\varepsilon_{r,eff}$ of the 1^{st} (dashed lines with markers) and 3^{rd} (solid lines with markers) mode by increasing the vertical (h^{step}_{port}) dimension of the modal port in CST, compared to the values obtained from EDC (black and red solid lines).

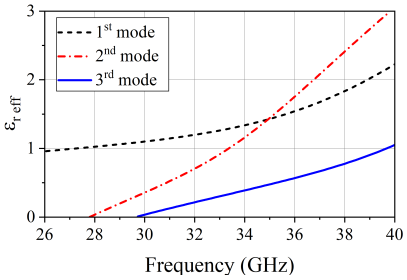

FIGURE 11. Effective dielectric constant $\varepsilon_{r,eff}$ of the higher order modes for the large CPW obtained with CST, setting $k^{step}_x = 4$, $k^{step}_y = 1.8$.

propagating in this structure can be done by considering three different dielectric regions (along the vertical direction) in the large CPW as shown in Fig. 8 [26]:

1) a dielectric slab with thickness h_{bulk} in the region under the signal line ($|x| < w_{line}/2$) and under the ground planes ($w_{line}/2 + w_{step} < |x| < w_{bulk}/2$), which is equivalent to a symmetric slab (along y) with thickness $2h_{bulk}$ with an electric wall in the symmetry plane. In fact, with a good approximation we can assume that the metal effectively used for the prototypes (i.e., gold) is equivalent to a perfect conductor acting as a "mirror" that doubles the structure (according to the well-known "Method of Images").
2) A symmetric (along y) dielectric slab with thickness h_{bulk} in the region comprised between the signal line and the ground planes ($w_{line}/2 < |x| < w_{line}/2+w_{step}$).
3) The air surrounding the structure, external to the lateral dimensions of the bulk ($|x| > w_{bulk}/2$).

In the previous description, we have simplified the structure in the y direction as the SiO_2 layer was missing, since its thickness (between 300 and 500 nm) is much smaller than the thickness of the Si substrate (i.e., 0.525 mm).

Considering z as the direction of propagation of the waves, the structure presents a double confinement for the EM field on the transverse plane. In order to better understand the effects of this confinement on the higher order modes and their coupling with the fundamental Quasi-TEM mode, the guided modes have been analyzed following the classical approach based on the Effective Dielectric Constant (EDC) method as in [27], which is not exactly rigorous but allows to correctly understand the modal behavior in the entire cross-section. In fact, in the EDC approach the fields are supposed to have only five components and the guiding effects in the y and x directions are analyzed in two successive steps.

Following the EDC method, the propagation constants of the higher order propagating modes, and consequently their effective dielectric constant values $\varepsilon_{r,eff}$, are evaluated. The obtained $\varepsilon_{r,eff}$ is shown in Fig. 9, from which we can see that in the analyzed frequency range three higher order modes appear, one of them always propagating and the others with cutoff at about 29 and 39 GHz.

The presence of such higher modes poses another question about the choice of the dimensions of the waveguide ports used in CST for the evaluation of the scattering matrix. To understand how the choice of the horizontal and vertical port dimensions could change the values of the modal propagation constant, a parametric analysis has been performed. To establish a relation between the height of the CST port and the distance between ground and line conductors as done for the horizontal dimension, we can set $h^{step}_{port} = h_{bulk} + k^{step}_y(w_{line} + 2w_{step})$. The effective dielectric constant $\varepsilon_{r,eff}$ for the first and third mode is shown in Fig. 10 by varying the height of the port ($k^{step}_y = 1, 1.2, 1.4, 1.6, 1.8$) and fixing its width. The second mode is not reported to keep the figure readable. The frequency range has been enlarged to better understand the behavior of the simulations carried out with CST.

From Fig. 10, it is clear that increasing the height of the port, the values obtained with CST tend to those obtained by

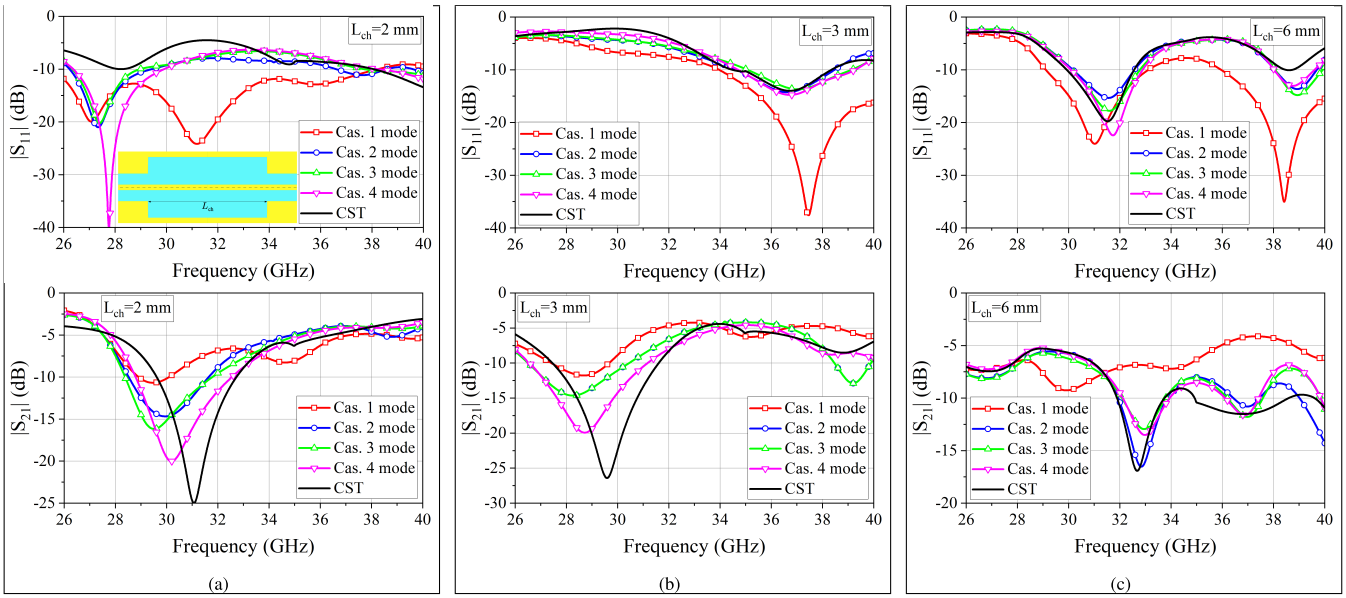

FIGURE 12. $|S_{11}|$ and $|S_{21}|$ comparison between cascade approach and CST evaluations for the double step without SRRs shown in the inset or enlarged in Fig. 3c, by varying the length L_{ch} of the channel and the number of modes considered in the cascade approach (red, blue, green, magenta: 1, 2, 3 or 4 modes, respectively).

the EDC method for $\varepsilon_{r,eff} > 1$ (the EDC values are shown with solid black and red lines).

We can choose a value of about $k_y^{step} = 1.8$ to obtain a good comparison in the analyzed band 26–40 GHz of our final simulations. Increasing k_y^{step} to higher values, a better agreement can be obtained, but too high values of k_y^{step} cause the propagation of "numerical" and unreal modes related only to the presence of the boundaries around the CST port. A similar parametric evaluation can be done for the width of the port and a value of $k_x^{step} = 4$ can be chosen to obtain a good comparison between EDC and CST values, as can be seen from Fig. 9 and Fig. 11, where $\varepsilon_{r,eff}$ obtained with CST is shown for the three higher order modes.

The main difference is related to the value of the frequency cutoff obtained with CST and the EDC method. In fact, it should be recalled that the actual CPW under study is an open waveguide. Hence, apart from the Quasi-TEM mode, the higher order modes must satisfy the guiding condition for an open waveguide: $k_0 \leq \beta \leq k_0\sqrt{\varepsilon_{r,\,bulk}}$ or $1 \leq \varepsilon_{r,eff} \leq \varepsilon_{r,\,bulk}$ [25, Ch. 14].

On the contrary, the higher order modes obtained with CST are related to the spatial limitations of the port boundary that implies the presence of enforcing boundary conditions typical of closed waveguides. For such structures, any higher order modes must satisfy $0 \leq \beta \leq k_0\sqrt{\varepsilon_{r,\,bulk}}$ or $0 \leq \varepsilon_{r,eff} \leq \varepsilon_{r,\,bulk}$ [28, Ch. 6]. Hence, there is a range of frequencies from the cutoff frequency of the CST mode to the actual cutoff frequency of the same mode in the dielectric open waveguide where the numerical approach of CST does not well reproduce the actual behavior of the EM field. On the other hand, another choice is not possible in CST and we need to maintain this discrepancy in this band. Comparing Fig. 9 with Fig. 11, the frequency ranges where this discrepancy appears are about 27.7–33 GHz for the 2^{nd} mode and 29.9–39.5 GHz for the 3^{rd} mode.

The same analysis has been applied also to the input port at $z = 0$ of Fig. 3c. In this case, only the Quasi-TEM mode is propagating because of the reduced distance between ground and line conductors.

In order to test the effects of the higher order modes, we have simulated the cascade of two steps as shown in the inset of Fig. 12 (or in Fig. 3c without SRRs), varying the distance L_{ch} between the steps and the number of modes traveling in the large CPW, by cascading the S-matrices of the "opening" and "closing" steps together with the phase shift due to the channel length L_{ch}: $S^{dstep} = S_{op}^{step} * S^{L_{ch}} * S_{cl}^{step}$. The cascade formula (1)-(4) must be upgraded to the case of multi-mode structure.

If we consider a generic reciprocal device with N_1 input and N_2 output modes, its scattering matrix can be divided into sub-blocks, as follows [24, Ch. A.4]:

$$S^a = \begin{bmatrix} [S_{11}^a]_{N_1\times N_1} & [S_{12}^a]_{N_1\times N_2} \\ [S_{12}^a]_{N_2\times N_1}^T & [S_{22}^a]_{N_2\times N_2} \end{bmatrix}. \tag{6}$$

In (6) T stands for transpose matrix. The global scattering matrix obtained with the cascade of the previous device with a second device characterized by the S^b matrix, with N_2 input and N_3 output modes, is $S^c = S^a * S^b$ with

$$[S_{11}^c]_{N_1\times N_1} = [S_{11}^a]_{N_1\times N_1} + [S_{12}^a]_{N_1\times N_2} \cdot \left[S_{11}^b\right]_{N_2\times N_2} \cdot \cdot \Delta_{N_2\times N_2} \cdot [S_{12}^a]_{N_2\times N_1}^T \tag{7}$$

$$[S_{12}^c]_{N_1\times N_3} = \left[S_{12}^b\right]_{N_3\times N_2} \cdot \Delta_{N_2\times N_2} \cdot [S_{12}^a]_{N_2\times N_1} \tag{8}$$

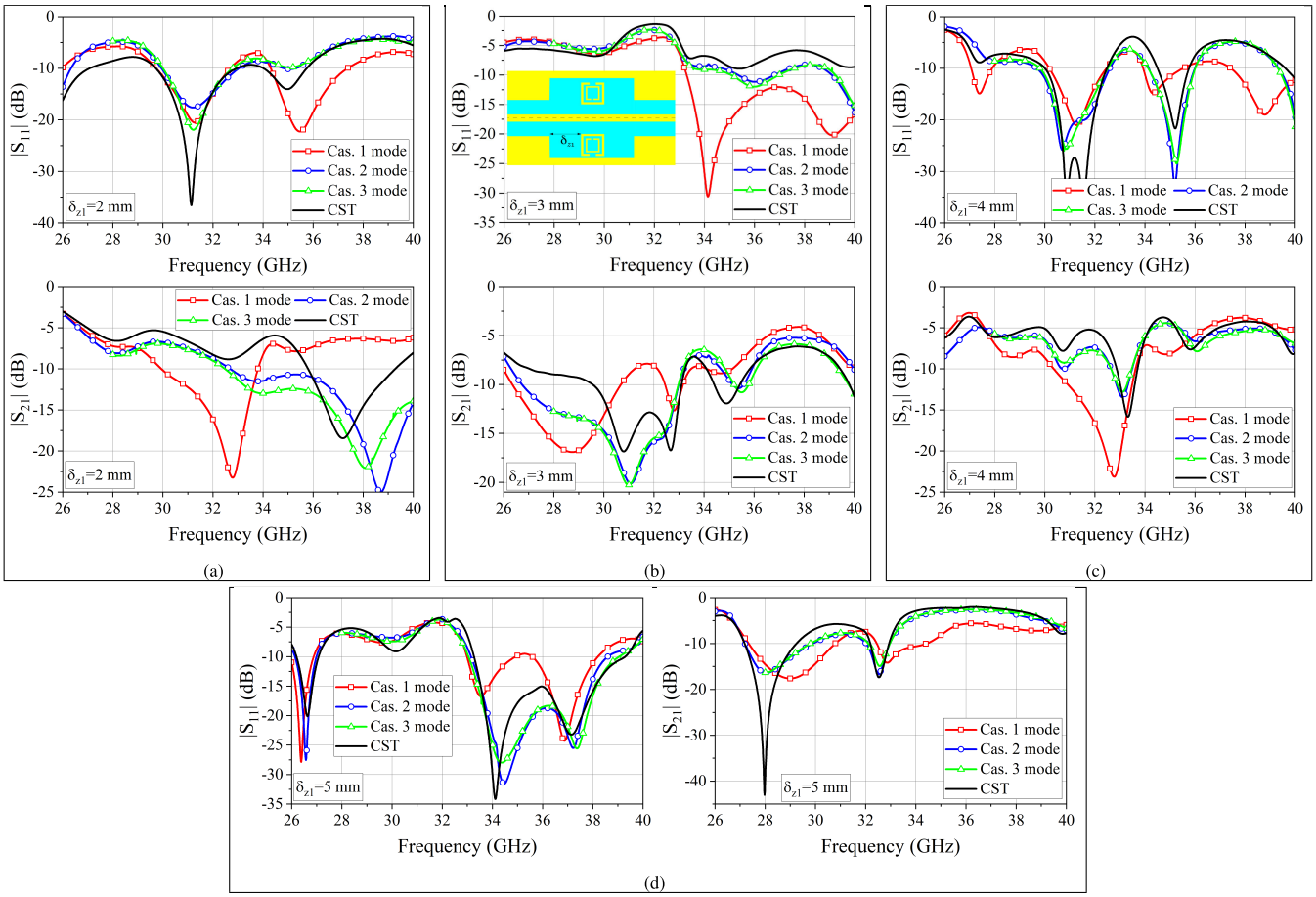

FIGURE 13. $|S_{11}|$ and $|S_{21}|$ for the structure with only one pair of SRRs shown in the inset or enlarged in Fig. 3c by varying the number of modes considered in the large CPW and the distance δ_{z1} between the SRRs and the steps. The numerical evaluations are obtained either with the cascade approach (magenta, red, blue: 1, 2, or 3 modes, respectively) or with CST (black solid lines).

$$\left[S_{22}^{c}\right]_{N_3\times N_3} = \left[S_{22}^{b}\right]_{N_3\times N_3} + \left[S_{12}^{b}\right]^{T}_{N_3\times N_2} \cdot \Delta_{N_2\times N_2} \cdot \left[S_{22}^{a}\right]_{N_2\times N_2} \cdot \left[S_{12}^{b}\right]_{N_2\times N_3} \tag{9}$$

$$\Delta_{N_2\times N_2} = \left\{[I]_{N_2\times N_2} - \left[S_{22}^{a}\right]_{N_2\times N_2} \cdot \left[S_{11}^{b}\right]_{N_2\times N_2}\right\}^{-1}. \tag{10}$$

$\left[S_{ij}^{a}\right]$, $\left[S_{ij}^{b}\right]$, $\left[S_{ij}^{c}\right]$ are the sub-blocks of matrices S^a, S^b, S^c as in (6). $[I]$ and $\cdot$ stand for identity matrix and for matrix multiplication, respectively. Finally, exponent -1 stands for matrix inversion.

Following the previous discussion about the presence of higher order modes in the large CPW, we have evaluated the scattering parameters for the "opening" step at $z = z_1$, $S_{\rm op}^{\rm step}$, in Fig. 3c, by considering four modes at the output section. The interested reader can found the plots of $S_{\rm op}^{\rm step}$ in Appendix C, Fig. 21. By applying the matrix cascade (7)-(10), we can obtain the scattering parameters of the double step without SRRs, namely $S^{\rm dstep}$. The obtained results are shown in Fig. 12. In these figures, the scattering parameters of the double step have been obtained by considering only the fundamental mode in the large CPW (red line with markers) or adding one higher mode at a time for a total of two (blue line with markers), three (green line with markers), and four (magenta line with markers) modes. Moreover, the results are compared with those obtained by the simulation of the overall double step calculated with CST (black line).

It is evident that the presence of the Quasi TEM mode alone (red lines) does not give correct results for any value of the channel length, if compared with respect to the CST simulations of the overall double step (black lines). Adding the first higher order mode (blue lines), the results becomes more accurate for channel length greater than 3-4 mm, especially for $|S_{11}|$. The results are in good agreement also for $|S_{21}|$, starting from $L_{\rm ch} = 6$ mm. We can also observe that the presence of the fourth mode (magenta lines) is quite useless for not too short channel, being very small the difference with respect to the case of only three modes. Hence, in the following we will consider the presence of only three modes in the large CPW. Finally, it should be noted a not perfect agreement in the higher part of the band for $|S_{21}|$. Probably, this is due to some radiation effect that cannot be taken into account in the approach based on the cascade of S-matrices.

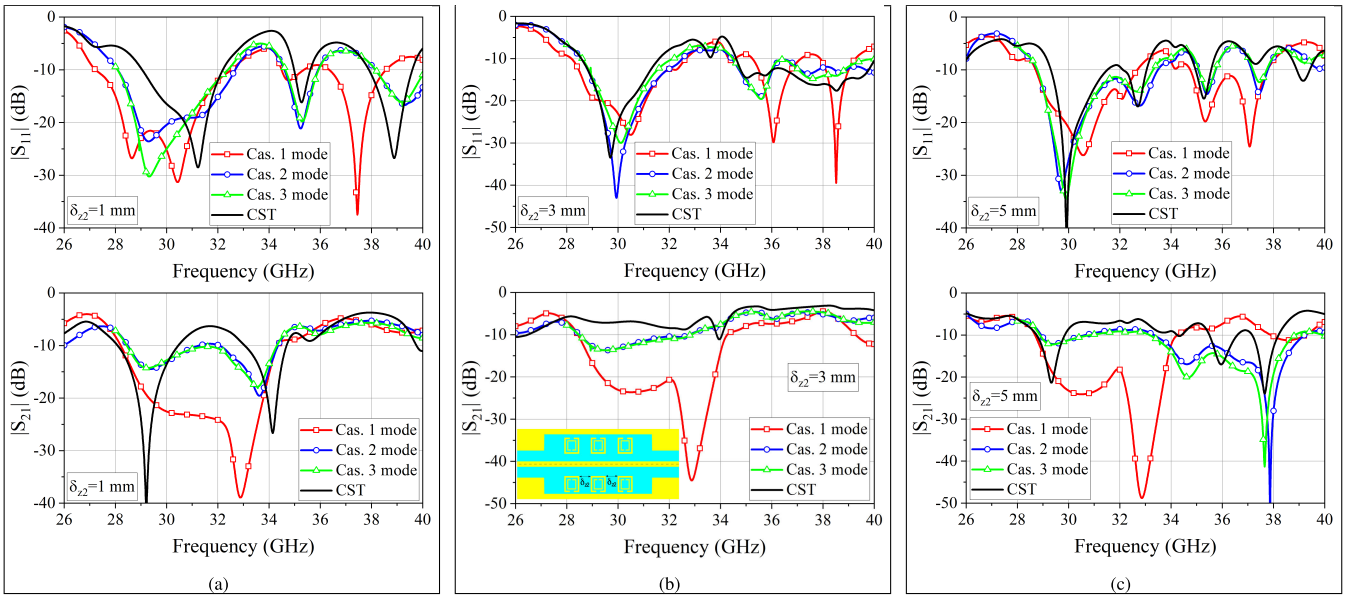

FIGURE 14. $|S_{11}|$ and $|S_{21}|$ for the structure with three pairs of SRRs shown in the inset or enlarged in Fig. 3c varying the distance δ_{z2} between them and setting $\delta_{z1} = 2$ mm. The numerical evaluations are obtained either with the cascade approach (magenta, red, blue: 1, 2, or 3 modes, respectively) or with CST (black solid lines).

TABLE 3. Run time comparison for the structure with one pair of SRRs resonators (Fig. 13).

Case	Cascade Approach Run Time	CST Run Time
$S_{\text{op}}^{\text{step}}$	6h 23m (with CST)	
S^{SRR}	3h 12m (with CST)	
Fig. 13a	3 s	1h 3m
Fig. 13b	3 s	1h 7m
Fig. 13c	3 s	1h 19m
Fig. 13d	3 s	2h 8m
whole Fig. 13	9h 35m ($S_{\text{op}}^{\text{step}}$+$S^{\text{SRR}}$) + 12 s (Fig. 13a-d)	7h 8m

TABLE 4. Run time comparison for the structure with three pairs of SRRs resonators (Fig. 14).

Case	Cascade Approach Run Time	CST Run Time
$S_{\text{op}}^{\text{step}}$	already evaluated for Fig. 13	
S^{SRR}	already evaluated for Fig. 13	
Fig. 14a	3 s	2h 52m
Fig. 14b	3 s	4h 8m
Fig. 14c	3 s	6h 5m
whole Fig. 14	9s	13h 5m

At this point, we can analyze the complete structure shown in Fig. 3c. To this aim, we need the multi-mode scattering parameters of one pair of SRRs in the large CPW that can be evaluated with CST with large ports (as previously discussed). The interested reader can found the plots of S^{SRR} in Appendix D, Fig. 22, for three input and three output modes.

The S parameters for the global structure containing only one pair of SRRs are shown in Fig. 13 by varying the number of modes considered in the large CPW and the distance δ_{z1} between the abrupt step and the pair of SRRs. By choosing three modes in the large CPW, the comparison seems good for the reflection coefficient and shows some differences in the transmission especially for the case when the SRR is very close to the abrupt step, where a strong interaction occurs between the "opening" step, the SRR, and the "closing" step. However, the cascade approach seems to be a good chance to obtain a reliable yet fast prediction of the behavior of the overall structure even in the presence of a multi-mode propagation. The run-time of the cascade approach is discussed in Tab. 3. In this case, the global time to obtain the data for the plots in Fig. 13 is greater than the direct evaluation with CST, but it should be noted that the simulation of any other configuration based on the same blocks requires only 3s against at least two hours with CST, making the cascade approach faster than the direct evaluation with CST.

Similarly, a case with three pairs of SRRs has been analyzed and the corresponding S parameters are shown in Fig. 14 by setting $\delta_{z1} = 2$ mm, varying the distance δ_{z2} between the pairs of SRRs and the number of modes. The comparison between the S parameters obtained with the cascade approach (with three modes) and the direct simulation of the global structure with CST are in good agreement, once we choose the right number of modes for the large CPW.

It should be noted that with the cascade approach we have obtained also the data for Fig. 14 at the cost of a few seconds ($S_{\text{op}}^{\text{step}}$ and S^{SRR} are the same for Figs. 13 and 14), while 13 hours are needed with CST, as shown in Tab. 4. Hence, the proposed method seems to be a winning strategy in the optimization process of complex structures from the EM point of view.

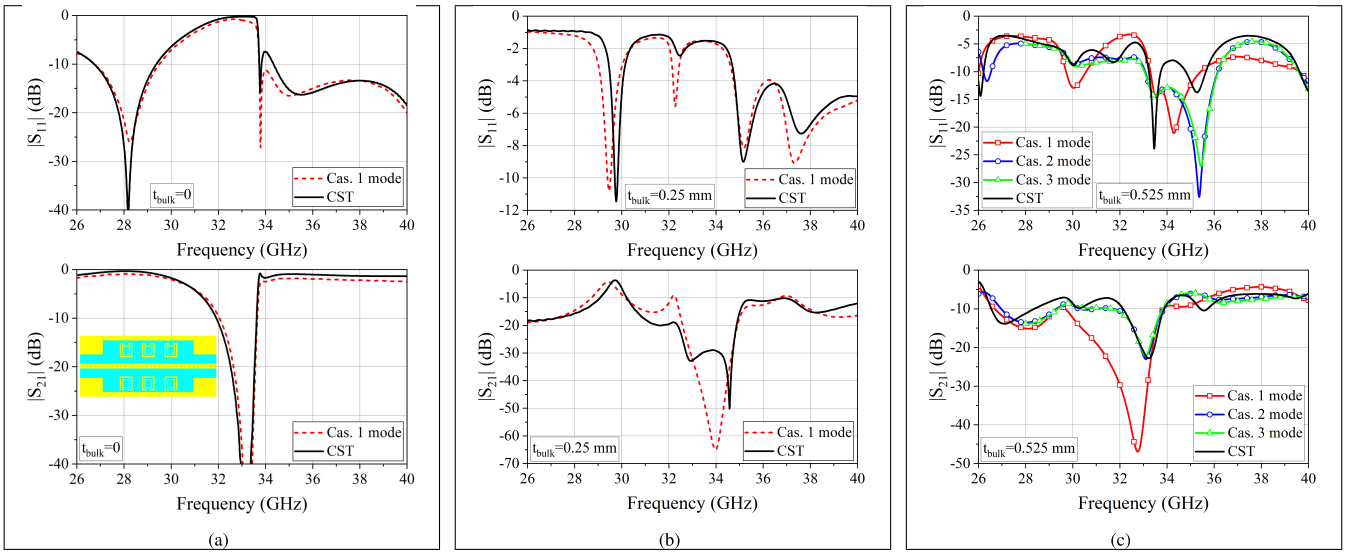

FIGURE 15. $|S_{11}|$ and $|S_{21}|$ for the structure with three pairs of SRRs shown in the inset or enlarged in Fig. 3c varying the thickness of the bulk substrate and the number of propagating modes either with cascade approach or with CST, setting $\delta_{z1} = 1$ mm, $\delta_{z2} = 2$ mm.

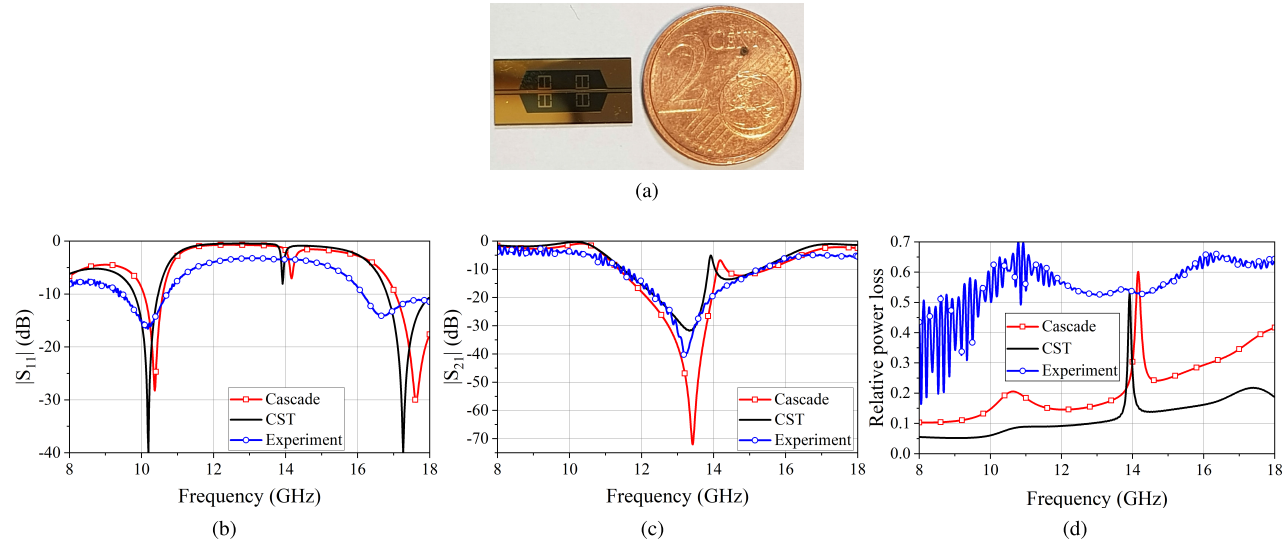

FIGURE 16. (a) Fabricated filter based on top-plane ELCs; (b)-(c) comparison between numerical and experimental results for $|S_{11}|$ and $|S_{21}|$; (d) comparison between losses for numerical and experimental results.

As a last numerical example, to emphasize the importance of taking into account the higher order modes, it can be considered the effect of the height of the dielectric beneath the conductor ($h_{\text{bulk}} = 0, 0.25, 0.525$ mm) in a device with three pairs of SRRs as the previous ones. The first case ($h_{\text{bulk}} = 0$ mm) is somehow ideal, where the coplanar is suspended in air with the pure TEM mode only propagating in the considered band. The results are shown in Fig. 16 and it is evident that propagation of higher order modes and their effects in the evaluation of the global scattering matrix are strictly related to the thickness of the substrate. In fact, only one mode can be used for a substrate thickness of up to 0.25 mm to obtain excellent agreement, while three modes must be taken into account to obtain a good comparison for higher values of substrate thickness.

III. EXPERIMENTAL RESULTS

A. FABRICATION

All the proposed filters were manufactured on high-resistivity silicon (HRSi) 4-inch wafers (resistivity $\rho \sim 10000\ \Omega \cdot cm$, <100> orientation). The first step was the thermal oxidation to create a thin layer (about 500 nm) of SiO_2. The fabrication process involved the use of one single mask for metal patterning by a lift-off process. For lithography, a double-layer photoresist technique was used: the first one was a LOR-type resist, and the second was AZ 5214.

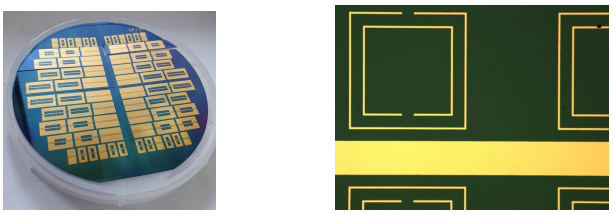

(a) (b)

FIGURE 17. Fabricated filters based on top-plane SRRs: (a) whole wafer; (b) detail with a SRR.

The metallization (gold) of the filters, with a total thickness of about 300 nm, was performed by e-beam evaporation. It is apparent that the manufacturing of the proposed DUTs is based on well-developed steps, suitable for CMOS-compatible technology and, hence, large-scale production. In fact, tens of filters were fabricated, with repeatable performance and the almost absence of defects.

B. ELCs IN THE TOP PLANE

We have fabricated the ELC-based filter shown in Fig. 16a characterized by a taper with the same dimensions as in Sec. II-B, with $\delta_{z1} = 1.325$ mm and $\delta_{z2} = 2.85$ mm. The filter has a stop-band behavior between 8 and 18 GHz, with a minimum of transmission around 13 GHz. The comparison among the cascade approach, the overall simulation with CST [10], and the experimental results are shown in Fig. 16b-16c. The numerical results show that the cascade approach is a very good approximation of the overall simulation made with CST, exhibiting only a little shift in the resonant frequencies, while the amplitudes of $|S_{11}|$ and $|S_{21}|$ are very similar. The differences between numerical and experimental results are principally related to the presence of higher losses in the experimental results, as shown in Fig. 16d where the power loss relative to 1 Watt is reported. Losses are likely due to several factors, like the contact resistance between the probe tips and the CPW, the tolerances in the electrical characteristics of the silicon substrate, the type of support (i.e., dielectric or metallic) on which the devices were measured, and most of all the radiation losses coming from the interactions between the fundamental mode and the radiating modes excited by the ELCRs.

C. SRRs IN THE TOP PLANE

The fabricated SRR-based filters shown in Fig. 17a-17b are characterized by an abrupt step and a variable number of pairs of SRRs (from 2 to 5 pairs), with the same dimensions as in Sec. II-C and $\delta_{z1} = 1$ mm and $\delta_{z2} = 0.8$ mm. The filters exhibit a high-pass behavior between 26 and 40 GHz, with a minimum of reflection between 36 and 37 GHz. The comparison among the cascade approach, the overall simulation with CST, and the experimental results are shown in Fig. 18. The numerical results show that the cascade approach (solid red lines) represents a good approximation of the complete CST simulations (solid black lines) for all the filters under consideration, especially for the reflection coefficient in the lower part of the considered band, and the agreement improves for pairs of SRRs not too close to the "opening" and "closing" steps. However, the minima of $|S_{11}|$ are very similar. The selected DUTs were those shown in Fig. Fig. 3b and Fig. 3c, as they can be measured on wafer in a straightforward way with standard probe tips for CPW structures, i.e., by putting the DUTs on any dielectric or metallic support. On the contrary, the filters of Fig. 3a require a more complicated measurement setup, since the meta-atoms are placed in the back side of the silicon substrate, meaning that any type of material in contact with them and other than air would strongly affect the propagation characteristics coming from the SRRs.

The comparison between the numerical (cascade or CST, red and black respectively) and the experimental results (solid blue lines) shows a good agreement in the reflection coefficient with a little shift of the resonant frequency, while some differences appear in the amplitudes of the transmission coefficient. These differences between numerical and experimental results are principally related to the presence of higher losses in the experimental results (contact resistance, actual losses of the substrate, radiation loss by radiating modes). Moreover, the experimental results have been obtained by placing the DUT on a PVC block, several centimeters thick, to ensure mechanical stability and a good alignment with respect to the probe tips for on-wafer measurements. For this reason, we have also simulated with CST the presence of such PVC substrate under the DUT, obtaining the results shown with solid green lines in Fig. 18. The numerical results obtained with CST with the presence of the PVC under the filters (green lines) show that the resonant frequency for $|S_{11}|$ moves toward lower frequencies with respect to the same results obtained with CST without the PVC (black lines). It can be seen that the experimental reflection resonant frequency is always between the corresponding resonances obtained in the numerical evaluations with air or PVC under the filters. Hence, we can assert that the presence of the PVC under the filters is able to change the position of the reflection resonant frequency. Moreover, the dielectric constant of the PVC used in the CST simulations has been chosen as a typical value (about 2.1), but we are not sure that the relative permittivity of the real PVC block attains that value. Anyway, we can expect that experimental and theoretical results can exhibit a very good agreement once the actual PVC dielectric constant is available and used in the numerical simulations. On the other hand, a correct evaluation of the PVC relative permittivity is out of the scope for this paper. Hence, we can conclude that the presence of the PVC in the experimental set up introduces uncertainties in the numerical simulations due to the not perfect knowledge of its dielectric constant to be used in CST. The numerical uncertainties can be lowered by simulating the same filter in the two opposite conditions (with and without the PVC under the filter), thus being almost sure that the experimental results will be between these two limiting cases.

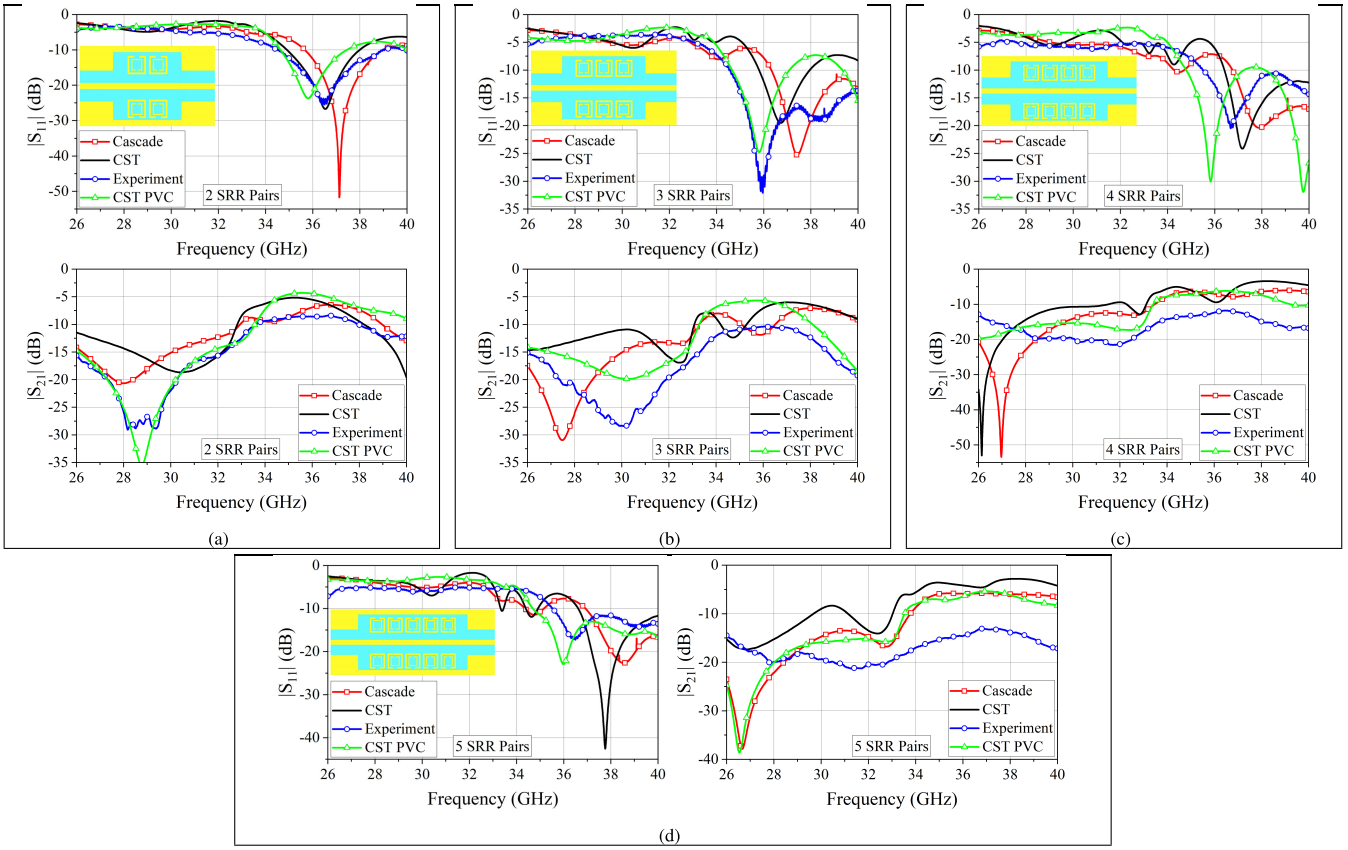

FIGURE 18. $|S_{11}|$ and $|S_{21}|$ for the fabricated SRR-based filters shown in Fig. 17 by varying the number of pairs of SRRs: (a) 2 pairs; (b) 3 pairs; (c) 4 pairs; (d) 5 pairs.

IV. CONCLUSION

In this paper, a general-purpose numerical procedure has been proposed and deeply analyzed to obtain a reliable prediction of the scattering parameters of CMOS-compatible ELC or SRR-based filters working in the X, Ku, K, and Ka bands. Each filter is an array of resonant meta-atoms in coplanar waveguide technology, obtained by cascading the scattering matrix of each block contained in the filter under study. The numerical analysis has proved that the results are excellent for structures where the fundamental TEM mode is propagating alone and that the approach could be a winning strategy to drastically reduce the computation time with respect to 3D EM simulations, which need to analyze the entire structure for each parametric evaluation. The proposed approach can be applied also to the case when higher order modes are propagating, thus giving a good prediction of the actual behavior with an acceptable margin of error due to unavoidable approximations. In this case, a preliminary modal analysis based on the application of the EDC method could be helpful to set the correct dimensions of the port used by the EM simulator. The final comparisons with the experimental results have shown that, apart from some experimental uncertainties, the cascade approach can be a good chance to develop a general-purpose and fast numerical procedure in the parametric study of complex passive devices with multimode propagation characteristics.

APPENDIX A
EVALUATION OF THE *S*-MATRIX FOR ONE PAIR OF SRRs IN THE BOTTOM PLANE

Referring to the inset in Fig. 19 or to Fig. 3a, the scattering parameters for the *S*-matrix for one pair of SRRs in the bottom plane are shown in Fig. 19. It should be noted the reflection properties of one pair of SRRs at about 30.2 GHz.

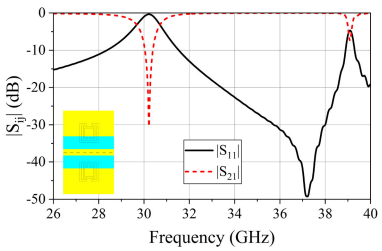

FIGURE 19. $|S_{11}|$ and $|S_{21}|$ for one back pair of SRRs (meta-atom), shown in the inset.

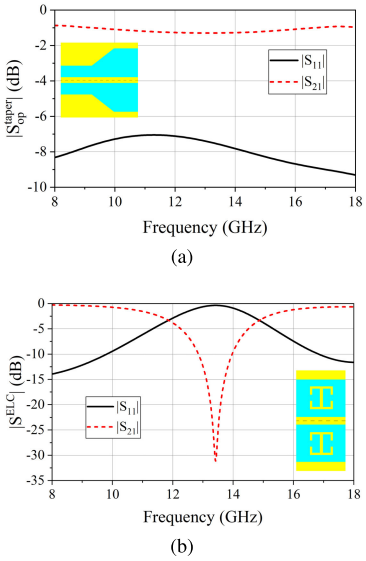

FIGURE 20. (a) $|S_{op}^{taper}|$ for the opening taper and (b) $|S^{ELC}|$ for one pair of ELCs (meta-atoms), shown in the insets.

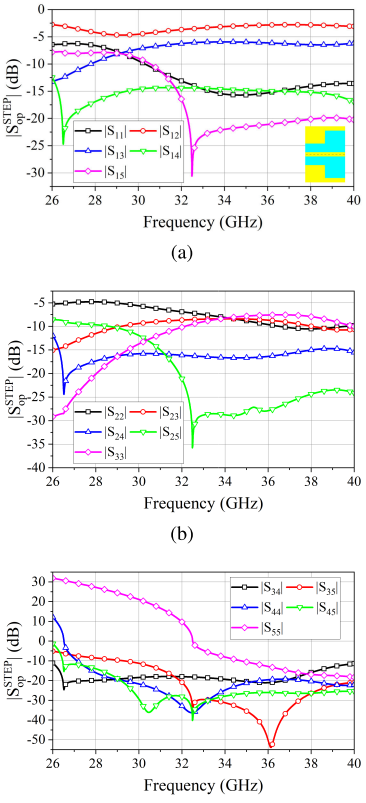

FIGURE 21. $|S_{op}^{step}|$ for the abrupt step opening shown in the inset, considering one input and four output modes. Index 1 refers to the input mode and indices 2, 3, 4, 5 to the four output modes.

APPENDIX B
EVALUATION OF THE *S*-MATRICES FOR THE OPENING TAPER AND ONE PAIR OF ELCs

Referring to the insets in Fig. 20 or to Fig. 3b, the scattering parameters for the S-matrix S_{op}^{taper} of the opening taper and the S-matrix S^{ELC} of one pair of ELCs are shown in Fig. 20.

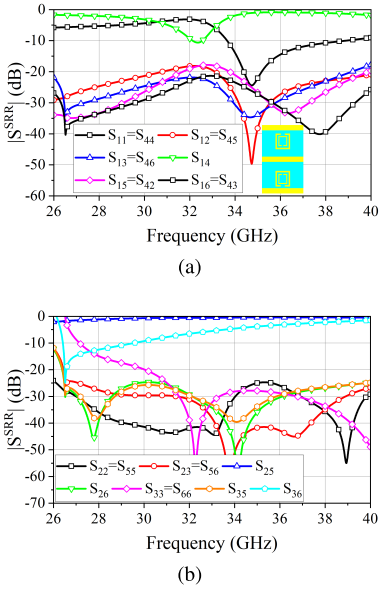

FIGURE 22. $|S^{SRR}|$ for one pair of SRRs shown in the inset, evaluated with CST, considering three input and output modes in the large CPW. Indices 1, 2, 3 refer to the three input mode and indices 4, 5, 6 to the three output modes.

It should be noted the reflection properties of one pair of ELCs at about 13.4 GHz.

APPENDIX C
EVALUATION OF THE MULTI-MODE *S*-MATRIX FOR THE ABRUPT STEP

Referring to the inset in Fig. 21 or to Fig. 3c, the multi-mode scattering parameters S_{op}^{step} for the abrupt step opening are shown in Fig. 21 in the band 26-40 GHz. It should not be surprising if some scattering parameters amplitudes are greater than 0 dB. This occurs for the higher order modes under cutoff, for which the constraint to be less than 0 dB is no more applicable [29], [30].

APPENDIX D
EVALUATION OF THE MULTI-MODE *S*-MATRIX FOR ONE PAIR OF SRRs IN THE LARGE CPW

Referring to the inset in Fig. 22 or to Fig. 3c, the multi-mode scattering parameters S^{SRR} for one pair of SRRs in the large CPW are shown in Fig. 22, for three input and three output modes.

REFERENCES

[1] M. Durán-Sindreu, P. Vélez, J. Bonache, and F. Martín, "Broadband microwave filters based on metamaterial concepts," in *Proc. Conf. Proc. ICECom, 20th Int. Conf. Appl. Electromagn. Commun.*, Sep. 2010, pp. 1–4.

[2] J. Naqui, M. Durán-Sindreu, and F. Martín, "Selective mode suppression in microstrip differential lines by means of electric-LC (ELC) and magnetic-LC (MLC) resonators," *Appl. Phys. A, Solids Surf.*, vol. 115, no. 2, pp. 637–643, May 2014.

[3] M. Gil, J. Bonache, J. Garcia-Garcia, J. Martel, and F. Martin, "Composite right/left-handed metamaterial transmission lines based on complementary split-rings resonators and their applications to very wideband and compact filter design," *IEEE Trans. Microw. Theory Techn.*, vol. 55, no. 6, pp. 1296–1304, Jun. 2007.

[4] A. Ebrahimi, W. Withayachumnankul, S. F. Al-Sarawi, and D. Abbott, "Dual-mode behavior of the complementary electric-LC resonators loaded on transmission line: Analysis and applications," *J. Appl. Phys.*, vol. 116, no. 8, Aug. 2014, Art. no. 083705.
[5] D. Schurig, J. J. Mock, and D. R. Smith, "Electric-field-coupled resonators for negative permittivity metamaterials," *Appl. Phys. Lett.*, vol. 88, no. 4, Jan. 2006, Art. no. 041109.
[6] J. Naqui, M. Durán-Sindreu, and F. Martín, "Differential and single-ended microstrip lines loaded with slotted magnetic-LC resonators," *Int. J. Antennas Propag.*, vol. 2013, pp. 1–8, 2013.
[7] J. Garcia-Garcia, J. Bonache, I. Gil, F. Martin, M. C. Velazquez-Ahumada, and J. Martel, "Miniaturized microstrip and CPW filters using coupled metamaterial resonators," *IEEE Trans. Microw. Theory Techn.*, vol. 54, no. 6, pp. 2628–2635, Jun. 2006.
[8] P. Nuangpirom, K. Ruangsiri, and S. Akatimagool, "Simulation based on wave iterative algorithm for CSRR metamaterial transmission line analysis," in *Proc. 17th Int. Conf. Electr. Engineering/Electronics, Comput., Telecommun. Inf. Technol. (ECTI-CON)*, Jun. 2020, pp. 595–598.
[9] H. Oraizi and S. Y. Torabi, "Novel application of a new metamaterial complementary electric LC resonator for the design of miniaturized sharp band-pass filters," *Int. J. RF Microw. Comput.-Aided Eng.*, vol. 23, no. 4, pp. 471–475, Jul. 2013.
[10] M. Aldrigo, L. Zappelli, A. Cismaru, M. Dragoman, S. Iordanescu, D. Mladenovic, C. Parvulescu, C. H. Joseph, D. Mencarelli, L. Pierantoni, and P. Russo, "Microwave coplanar band-stop filters based on electric-LC resonators: Systematic numerical approach and experimental validation," *J. Comput. Electron.*, vol. 22, no. 4, pp. 1031–1036, Aug. 2023, doi: 10.1007/S10825-023-02041-9.
[11] R. Dudley and M. Fiddy, *Engineered Materials and Metamaterials: Design and Fabrication*. Bellingham, WA, USA: SPIE, 2017.
[12] W. Cai and V. Shalaev, *Optical Metamaterials: Fundamentals and Applications*. New York, NY, USA: Springer, 2009.
[13] Y. Dong and T. Itoh, "Metamaterial-based antennas," *Proc. IEEE*, vol. 100, no. 7, pp. 2271–2285, Jul. 2012.
[14] S. B. Glybovski, S. A. Tretyakov, P. A. Belov, Y. S. Kivshar, and C. R. Simovski, "Metasurfaces: From microwaves to visible," *Phys. Rep.*, vol. 634, pp. 1–72, May 2016.
[15] G. Perrakis, A. C. Tasolamprou, G. Kenanakis, E. N. Economou, S. Tzortzakis, and M. Kafesaki, "Combined nano and micro structuring for enhanced radiative cooling and efficiency of photovoltaic cells," *Sci. Rep.*, vol. 11, no. 1, p. 11552, Jun. 2021.
[16] M. Chen, M. Kim, A. M. H. Wong, and G. V. Eleftheriades, "Huygens' metasurfaces from microwaves to optics: A review," *Nanophotonics*, vol. 7, no. 6, pp. 1207–1231, Jun. 2018.
[17] A. C. Tasolamprou, E. Skoulas, G. Perrakis, M. Vlahou, Z. Viskadourakis, E. N. Economou, M. Kafesaki, G. Kenanakis, and E. Stratakis, "Highly ordered laser imprinted plasmonic metasurfaces for polarization sensitive perfect absorption," *Sci. Rep.*, vol. 12, no. 1, p. 19769, Nov. 2022.
[18] T. A. Tsiftsis, C. Valagiannopoulos, H. Liu, A. A. Boulogeorgos, and N. I. Miridakis, "Metasurface-coated devices: A new paradigm for energy-efficient and secure 6G communications," *IEEE Veh. Technol. Mag.*, vol. 17, no. 1, pp. 27–36, Mar. 2022.
[19] C. Liaskos et al., "XR-RF imaging enabled by software-defined metasurfaces and machine learning: Foundational vision, technologies and challenges," *IEEE Access*, vol. 10, pp. 119841–119862, 2022.
[20] M. Di Renzo, F. H. Danufane, and S. Tretyakov, "Communication models for reconfigurable intelligent surfaces: From surface electromagnetics to wireless networks optimization," *Proc. IEEE*, vol. 110, no. 9, pp. 1164–1209, Sep. 2022.
[21] M. Poulakis, "Metamaterials could solve one of 6G's big problems [industry view]," *Proc. IEEE*, vol. 110, no. 9, pp. 1151–1158, Sep. 2022.
[22] M. Di Renzo and A. I. Aravanis, "Catching the 6G wave by using metamaterials," in *Shaping Future 6G Networks*. Hoboken, NJ, USA: Wiley, 2021, ch. 6, pp. 69–87.
[23] F. Bilotti, A. Toscano, L. Vegni, K. Aydin, K. B. Alici, and E. Ozbay, "Equivalent-circuit models for the design of metamaterials based on artificial magnetic inclusions," *IEEE Trans. Microw. Theory Techn.*, vol. 55, no. 12, pp. 2865–2873, Dec. 2007.
[24] D. Budimir, *Generalized Filter Design by Computer Optimization*. London, U.K.: Artech House, 1998.
[25] S. Ramo, J. Whinnery, and T. Van Duzer, *Fields and Waves in Communication Electronics*. Hoboken, NJ, USA: Wiley, 1994.
[26] M. Riaziat, R. Majidi-Ahy, and I.-J. Feng, "Propagation modes and dispersion characteristics of coplanar waveguides," *IEEE Trans. Microw. Theory Techn.*, vol. 38, no. 3, pp. 245–251, Mar. 1990.
[27] W. V. McLevige, T. Itoh, and R. Mittra, "New waveguide structures for millimeter-wave and optical integrated circuits," *IEEE Trans. Microw. Theory Techn.*, vol. MTT-23, no. 10, pp. 788–794, Oct. 1975.
[28] R. Collin, *Field Theory of Guided Waves*. Piscataway, NJ, USA IEEE Press, 1990.
[29] A. Morini and T. Rozzi, "On the definition of the generalized scattering matrix of a lossless multiport," *IEEE Trans. Microw. Theory Techn.*, vol. 49, no. 1, pp. 160–165, Jan. 2001.
[30] L. Zappelli, "An equivalent circuit for discontinuities exciting evanescent accessible modes," *IEEE Trans. Microw. Theory Techn.*, vol. 60, no. 5, pp. 1197–1209, May 2012.

M. ALDRIGO (Senior Member, IEEE) received the Ph.D. degree in electronic engineering, telecommunications, and information technology from the Faculty of Engineering, University of Bologna, Bologna, Italy, in 2014. Since January 2022, he has been a Principal Researcher II with IMT-Bucharest, Voluntari, Romania. He has coauthored more than 90 papers in ISI ranked journals and conferences. His main research interests include the electromagnetic simulation and experimental characterization of high-frequency systems for wireless/energy-harvesting applications embedding carbon-based, 2D, and nanoscale ferroelectric materials. He serves or has served as reviewer/guest editor for many journals and as (co-)chair in international conferences.

L. ZAPPELLI (Member, IEEE) received the M.S. (summa cum laude) and Ph.D. degrees in electronic engineering from the University of Ancona, Ancona, Italy, in 1986 and 1991, respectively. Since 1988, he has been with the Department of Information Engineering, Università Politecnica delle Marche (UnivPM), Ancona, where he is currently an Assistant Professor. His research interests include microwaves, electromagnetic compatibility, phased array antennas, frequency-selective surfaces, and microwave equivalent circuits.

A. CISMARU received the master's and Ph.D. degrees in physics from the Physics Faculty, University of Bucharest, in 2000 and 2008, respectively. Since 2022, she has been a Principal Researcher I with IMT-Bucharest, Romania. Her main expertise is the design and fabrication of EMBG-based devices for microwave applications, CNT-based sensors for the detection of "greenhouse" type gases (CO, CO2, and CH4), SAW and FBAR characterization for microwave applications, and microphysics characterization using white-light interferometer (WLI). She has coauthored more than 60 scientific papers in ISI-ranked journals and conferences.

M. DRAGOMAN received the Ph.D. degree in electronics from the University "Politehnica" Bucharest, Bucharest, Romania, in 1991. He followed Postdoctoral studies with Duisburg University, Duisburg, Germany. He is currently a Senior Researcher I with IMT-Bucharest, Voluntari, Romania. He has coauthored more than 250 scientific papers in ISI ranked journals and conferences, and six monographies. From 1992 to 1994, he was a recipient of the Humboldt Fellowship Award. He was awarded the Gheorghe Cartianu prize of the Romanian Academy, in 1999.

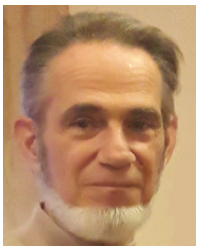

S. IORDANESCU (Life Member, IEEE) graduated from the Faculty of Electronics and Telecommunications, Polytechnic Institute of Bucharest, Bucharest, Romania, in 1972, and the Ph.D. degree in electronic engineering from the University "Politehnica" Bucharest, Bucharest, Romania, in 2000. Since 2015, he has been a Senior Researcher with IMT-Bucharest, Voluntari, Romania. He is the author of more than 120 scientific papers in peer-reviewed journals and conferences. His research interests include microwave SAW filter and sensor design, the characterisation of dielectric and ferroelectric materials, and the design of various microwave and millimetre wave circuits. He was a recipient of the Tudor Tanasescu Romanian Academy Award (with team), in 2003.

D. MLADENOVIC is currently pursuing the Ph.D. degree in physics with the Faculty of Physics, University of Bucharest, Romania. He is a Researcher with IMT-Bucharest, Romania.

C. PARVULESCU received the Ph.D. degree from the Faculty of Electronics, Telecommunications, and Information Technology, University "Politehnica" Bucharest, Bucharest, Romania, in 2015. He is currently a Technological Development Engineer III with the Laboratory of Technological Processing, IMT-Bucharest, Romania. He has professional experience in photolithography processes, processing and characterization of photosensitive films, wet etching, nano-imprint lithography processes, bonding processes, microfabrication processes for microfluidics, sensors, opto-microelectronics devices, and microwaves. He has coauthored more than 35 papers in international journals and eight national patents. He has been/is coordinator/team member in several national projects.

D. VASILACHE received the Ph.D. degree from the University "Politehnica" Bucharest, Bucharest, Romania. He is currently a Senior Researcher II with IMT-Bucharest, Voluntari, Romania. He is the author of more than 150 papers (33 in ISI ranked journals). His research interests include MEMS and NEMS design, manufacturing and encapsulation, thin films deposition and patterning, masks design, and manufacturing.

C. H. JOSEPH (Member, IEEE) received the B.Sc. degree in physics from the St. John's College, Tirunelveli, India, in 2007, the M.Sc. degree in physics from The American College, Madurai, India, in 2010, and the Ph.D. degree in electronic engineering from the University of Rome "Tor Vergata," Rome, Italy, in 2016. From 2017 to 2018, he was an institute Postdoctoral Researcher with the Department of Physics, IIT Madras, Chennai, India. Since 2018, he has been a Researcher with the Department of Information Engineering, Università Politecnica delle Marche (UnivPM), Ancona, Italy. His current research interests include nanoscale characterization of advanced materials and biological structures using scanning microwave microscopy (SMM) technique, nanoelectronics, microwave/millimeter wave, and Sub-THz metamaterials device modeling and design. He was a recipient of the "Marie Curie Fellowship" and worked as an Early-Stage Researcher with the National Research Council (CNR-IMM), Rome, Italy, from 2013 to 2016.

D. MENCARELLI (Member, IEEE) received the Laurea and Ph.D. degrees in electronic and telecommunication engineering from Università Politecnica delle Marche (UnivPM), Ancona, Italy, in 2002 and 2005, respectively. Since 2014, he has been an Assistant Professor with the Department of Information Engineering, UNIVPM. His research interests include coherent charge transport in low dimensional systems, photonic crystals, nano-field effect transistors (nano-FET), planar slot array antennas and microwave components, scanning probe microscopy (SPM), optomechanics, and phononic devices. He is currently a member of the IEEE MTT'S Speaker Bureau, the Vice Chair of the MTT TC 8 Technical Committee "RF Nanotechnology," an Associate Editor of the IEEE TRANSACTIONS OF NANOTECHNOLOGY and *Journal of Computational Electronics*.

L. PIERANTONI (Senior Member, IEEE) received the Laurea degree (summa cum laude) in electronic engineering and the Ph.D. degree in electromagnetics from the University of Ancona, Ancona, Italy, in 1988 and 1993, respectively.

From 1996 to 1999, he was a Senior Research Scientist with the Technical University of Munich, Munich, Germany. He is currently a Full Professor of electromagnetic fields with Università Politecnica delle Marche (UnivPM), Ancona. His research interests include the investigation of the combined Maxwell-quantum transport phenomena in nano-materials/devices, the development of computational techniques for the multiphysics modeling of nano-to-meso-scale devices/systems, and atomistic (ab initio) simulations of novel and smart materials.

Dr. Pierantoni is a Founder and the First Chair of the MTT-S RF Nanotechnology Technical Committee. He is also an IEEE MTT-S Distinguished Microwave Lecturer (DML), from 2012 to 2014, IEEE MTT-S DML Emeritus, from 2015 to 2016, IEEE Nanotechnology Council (NTC), Distinguished Lecturer, from 2015 to 2016, and IEEE TNANO as a Senior Editor. He is a Vice-President of the NTC for the educational activities. He has got 12 European granted projects.

P. RUSSO (Member, IEEE) received the Ph.D. degree in electronic engineering from the Polytechnic University of Bari, Bari, Italy, in April 1999.

From January 2005 to July 2019, she was an Assistant Professor with Università Politecnica delle Marche (UnivPM), Ancona, Italy, where she was appointed as an Associate Professor, in August 2020. She teaches antenna design and fundamental of electromagnetics. Her main research interests include the application of numerical modeling to EMC problems, antenna problems, plasma antennas, and electromagnetic sensors.

Dr. Russo is a member of the Italian Electromagnetic Society (SIEm) and the Scientific Board of Italian Center for the study of the interactions between electromagnetic fields and biosystem (ICEmB).

Open Access funding provided by 'Università Politecnica delle Marche' within the CRUI CARE Agreement